

CMB lensing from early-formed dark matter halos

Katsuya T. Abe^{1,*} and Hiroyuki Tashiro²

¹Center for Frontier Science, Chiba University, 1-33 Yayoi-cho, Inage-ku, Chiba 263-8522, Japan

²Center for Education and Innovation, Sojo University, Ikeda, Nishi-ku, Kumamoto, 860-0082 Japan

Some theoretical models for the early universe predict a spike-type enhancement in the primordial power spectrum on a small scale, which would result in forming early-formed dark matter halos (EFHs). In this work, we study the CMB lensing effect, considering the existence of EFHs, and investigate the potential to probe the EFHs and the primordial perturbations on scales smaller than 1Mpc. We numerically calculate the angular power spectrum of the lensing potential and the lensed CMB anisotropy of temperature, E-mode, and B-mode polarization, including the nonlinear effects of EFHs. We find the possibility that the lensed CMB temperature anisotropy is significantly enhanced on small scales, $\ell > 1000$, and could be tested by component decomposition of observed signals through multi-frequency observations. Through the calculation with different models of the spiky-type power spectrum, we demonstrate that the accurate measurements of the CMB lensing effect would provide insight into the abundance of EFHs within the limited mass range around $10^{12}M_{\odot}$ and the primordial power spectrum on the limited scales around $k \sim 1\text{Mpc}^{-1}$. In particular, we find that the existence of such EFHs can amplify the lensed anisotropy of CMB B-mode polarization even on large scales, $\ell < 100$, as the overall enhancement by $\sim 10\%$ level compared to the standard structure formation model without EFHs. Therefore, future CMB measurements such as the LiteBIRD satellite can probe the existence of the EFHs and the spike-type primordial power spectrum through the precise measurement of the large-scale CMB B-mode polarization.

I. INTRODUCTION

The universe exhibits rich hierarchical structures spanning vast ranges of magnitude, *e.g.*, galaxy and galaxy clusters. The seeds of such hierarchical structures are called primordial perturbations. Precise measurements of cosmic microwave background (CMB) and large-scale structures have been achieved to measure the amplitude of primordial perturbations on larger scales than $\mathcal{O}(0.1-1)$ Mpc [1–7]. They have also allowed us to reveal their several statistical features on large scales, which remarkably align with predictions derived from the simplistic inflation scenario. Conversely, the measurement of perturbations on smaller scales has encountered significant challenges, primarily due to the nonlinear effects associated with the formation of structures, although that is crucial to further understanding the inflationary mechanism. Various scenarios, including inflation and dark matter, have proposed different types of small-scale fluctuation spectra. For instance, several inflationary scenarios propose the occurrence of a spike-type enhancement, such as those found in single-field or multi-field models featuring hybrid or double inflation [8–10]. Besides, particle production during inflation [11–13] and specific thermal histories such as an early matter-dominated era [14–17] or an era dominated by a fast-rolling scalar field [18] could generate a spike-type enhancement in the primordial power spectrum.

Such significantly enhanced small-scale fluctuations might play an essential role in forming cosmic structures and can largely impact cosmological signals. For

example, the spike-type small-scale fluctuations predict the formation of primordial black holes and early-formed dark matter halos (EFHs)¹. Here, we investigate the scenario in which the power of fluctuations is still linear and focus on only EFHs. This scenario has been examined and constrained through diverse cosmological signals. For instance, the energetic emission through DM annihilation from EFHs is one of the examples. So far, the gamma-ray emission signal [19–25] and the following effect on cosmic reionization [26–29] have been investigated assuming that the dark matter is of particle such as the weakly interacting massive particle [30–32]. Non-detection of such energetic signals in Fermi-LAT [33] and the observational value of the Thomson scattering optical depth put constraints on the abundance of EFHs and the small-scale primordial scalar perturbation as $\mathcal{A}_{\zeta} < 10^{-7}$ for $10 \text{ Mpc}^{-1} < k < 10^8 \text{ Mpc}^{-1}$. In addition, there are several works to examine the abundance in independent ways of the DM nature. For example, Refs. [22, 34] studied their gravitational lensing effect [22, 34], and Refs. [35–37] studied their baryonic effects. Both works have provided meaningful limits on the abundance of EFHs and also the small-scale primordial scalar perturbation, *e.g.*, $\mathcal{A}_{\zeta} \lesssim 10^{-7}$ for $1 \text{ Mpc}^{-1} \lesssim k \lesssim 100 \text{ Mpc}^{-1}$ and $\mathcal{A}_{\zeta} \lesssim 10^{-6}$ on $100 \text{ Mpc}^{-1} \lesssim k \lesssim 1000 \text{ Mpc}^{-1}$.

In this work, we focus on investigating the impact of these fluctuations on the weak gravitational lensing effect of CMB, commonly referred to as the CMB lensing

¹ In previous works, EFHs with the spike-type excess have been discussed in the context of ultracompact minihalos (UCMHs). However, UCMH originally indicates objects which gravitationally collapse near and by $z = 1000$, so that requiring $\delta\rho/\rho \gtrsim 10^{-3}$. On the contrary, we here do not limit the formation redshift of DM halos. Thus, we call them just EFHs.

* kabe@chiba-u.jp

effect. Understanding the influence of small-scale fluctuations on the CMB lensing effect is important to probe EFHs and primordial scalar perturbations on small scales in light of forthcoming observations of CMB anisotropies, particularly measurements of small-scale CMB temperature fluctuations, polarization modes, and large-scale polarization B-modes.

This paper is organized as follows. Section II describes the additional power spectrum and the features of formed EFHs. In Sect. III, we discuss the CMB lensing effects considering the nonlinear effects of EFHs. In Sect. IV, we calculate the lensed anisotropies of the CMB temperature, E-mode, and B-mode polarization, including the nonlinear effects of EFHs and discuss the signals compared to the observation data. In Sect. V, we conclude this paper.

Throughout this paper, we will assume a flat Λ CDM cosmology and fix the cosmological parameters to the Planck 2018 best-fits [1], ($h = 0.677$, $\Omega_b h^2 = 0.0224$, $\omega_{\text{cdm}} = 0.120$, $\ln(10^{10} \mathcal{A}_\zeta) = 3.05$, $n_s = 0.967$, and $\tau_{\text{reio}} = 0.0544$)

II. EARLY-FORMED DARK MATTER HALOS FROM THE SPIKE-TYPE PERTURBATIONS

Our aim of this paper is to investigate the potential of the CMB gravitational lensing to probe the EFHs and their origin, *i.e.*, primordial perturbations on scales smaller than 1 Mpc. Therefore, in addition to the standard almost-scale-invariant power spectrum, we assume the presence of a spike-type power spectrum at a specific small scale in the primordial perturbation \mathcal{P}_ζ ,

$$\mathcal{P}_\zeta = \mathcal{P}_\zeta^{\text{st}}(k) + \mathcal{P}_\zeta^{\text{add}}(k). \quad (1)$$

Here $\mathcal{P}_\zeta^{\text{st}}(k)$ denotes the standard almost-scale-invariant power spectrum, $\mathcal{P}_\zeta^{\text{st}}(k) = \mathcal{A}_\zeta (k/k_p)^{n_s}$ with the amplitude $\mathcal{A}_\zeta \sim 2.1 \times 10^{-9}$, the spectrum index $n_s = 0.967$, and the pivot scale $k_p = 0.05 \text{Mpc}^{-1}$, according to Ref. [1].

In Eq. (1), $\mathcal{P}_\zeta^{\text{add}}(k)$ is the additional spike-type power spectrum, which is given by

$$\mathcal{P}_\zeta^{\text{add}}(k) = \frac{\mathcal{A}_\zeta^{\text{add}}}{\sqrt{2\pi}\sigma_{\text{sp}}} \exp\left[-\frac{1}{2}\left(\frac{\ln(k) - \ln(k_{\text{sp}})}{\sigma_{\text{sp}}}\right)^2\right], \quad (2)$$

where $\mathcal{A}_\zeta^{\text{add}}$ is an amplitude of the additional spike-type power spectrum, k_{sp} is a comoving wave number representing the peak scale of the spike, and σ_{sp} is a logarithmic width of the spike. In this work, we fix $\sigma_{\text{sp}} = 0.1$ for simplicity. Thus, in the paper, we describe the additional spike-type power spectrum by using two parameters, $(k_{\text{sp}}, \mathcal{A}_\zeta^{\text{add}})$.

The existence of the spike-type primordial perturbations provides an impact on the structure formation history of the universe. The spike-type primordial perturbation can induce a large amplitude in the matter density fluctuations and lead to the early formation of gravitational collapse objects, which are called EFHs. The

EFHs produced by the spike-type power spectrum have been investigated in several works [24, 25]

The typical mass of EFHs produced by the spike-type fluctuations on a scale of k_{sp} is given by

$$M_h = \frac{4\pi}{3} \bar{\rho}_m \left(\frac{2\pi}{k_{\text{sp}}}\right)^3 \sim 4.4 \times 10^{10} M_\odot \times \left(\frac{k_{\text{sp}}}{10 \text{Mpc}^{-1}}\right)^{-3}, \quad (3)$$

where $\bar{\rho}_m$ is the comoving mean matter density. Through this equation, k_{sp} can be connected to M_h directly.

In Figure 1, we show the spike-type power spectra represented in Eq. (2) with the scale-invariant spectrum. We take two sets of spike-type power spectrum parameters, $(k_{\text{sp}}[\text{Mpc}^{-1}], \mathcal{A}_\zeta^{\text{add}}) = (3.4, 10^{-6})$ and $(16.0, 10^{-7})$, which are shown in blue and orange lines, respectively. According to Eq. (3), these two values of k_{sp} correspond to the mass of the EFHs, $10^{12} M_\odot$ and $10^{10} M_\odot$, respectively. The grey-shaded region in Fig. 1 indicates the scales in which cosmological observation has already measured the primordial perturbations. In the scales below the shaded region, there are only subtle constraints through measurements of CMB distortion by COBE/FIRAS [38, 39], $\mathcal{P}_\zeta \lesssim 10^{-5}$, and non-detection of PBHs, $\mathcal{P}_\zeta \lesssim 10^{-2}$ [40]. Thus, there is room for the existence of the spike-type primordial perturbations as shown in Fig. 1.

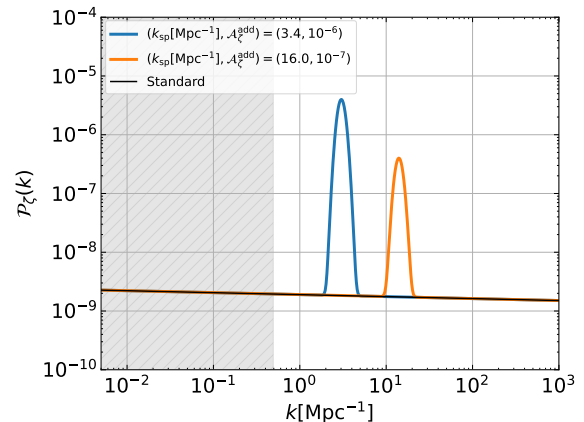


FIG. 1. The primordial power spectrum considered in this work. While a black solid line shows the standard almost-scale-invariant power spectrum with the amplitude of $\mathcal{A}_\zeta \sim 2.1 \times 10^{-9}$, coloured solid lines represent the ones with the additional spike-type power spectrum given by Eq. (2). A Location and amplitude of the spike are controlled by k_{sp} and $\mathcal{A}_\zeta^{\text{add}}$. We plot the spectrum with two parameter sets, $(k_{\text{sp}}[\text{Mpc}^{-1}], \mathcal{A}_\zeta) = (3.4, 10^{-6})$ and $(16.0, 10^{-7})$ in blue and orange solid lines. The grey-shaded region indicates the scales at which other cosmological measurements can probe.

Now we discuss the number density of EFHs for a given spike-type power spectrum. Since we here consider the EFHs formed from the spike-type fluctuations, the number density can be evaluated by employing the peak the-

ory [41, hereafter BBKS] as

$$n(M_h, z) = \frac{k_{\text{sp}}^3}{(2\pi)^2 3^{3/2}} \int_{\delta_c/S_{\text{mat}}^{1/2} D_+(z)}^{\infty} e^{-\nu^2/2} f(\nu) d\nu, \quad (4)$$

where $\delta_c = 1.69$ is the linear density threshold for collapse, S_{mat} is the present mass variance of the matter density fluctuation, $D_+(z)$ is the linear growth rate at z , and $f(\nu)$ is the function which is defined as

$$\begin{aligned} f(\nu) = & \frac{1}{2} \nu (\nu^2 - 3) \left(\text{erf} \left[\frac{1}{2} \sqrt{\frac{5}{2}} \nu \right] + \text{erf} \left[\sqrt{\frac{5}{2}} \nu \right] \right) \\ & + \sqrt{\frac{2}{5\pi}} \left\{ \left(\frac{8}{5} + \frac{31}{4} \nu^2 \right) \exp \left[-\frac{5}{8} \nu^2 \right] \right. \\ & \left. + \left(-\frac{8}{5} + \frac{1}{2} \nu^2 \right) \exp \left[-\frac{5}{2} \nu^2 \right] \right\}. \end{aligned} \quad (5)$$

Although the mass of EFHs grows through, *e.g.*, the gas accretion and the merger, the mass growth rate would not be large such as logarithmically, $M_h \propto \log a$ [25]. Therefore, we neglect the mass increment of EFHs and assume that the mass of EFHs can be fixed to the mass calculated in Eq. (3) throughout this paper.

The present mass variance S_{mat} is calculated from the power spectrum of the primordial perturbations in

$$S_{\text{mat}}(M_h) = \int d \log k \mathcal{P}_\zeta(k) T^2(k) \tilde{W}_k^2(kR(M_h)), \quad (6)$$

where $\tilde{W}_k(x)$ represents the Fourier function of the window function, $R(M_h)$ corresponds to the comoving scale that encloses the mass M_h in the background matter density $\Omega_m \rho_{\text{cri}}$, and $T(k)$ denotes the transfer function for the linear matter density fluctuations, which can be obtained from CAMB [42]. Using this notation, the dimensionless linear matter density power spectrum at the present epoch is described as

$$\mathcal{P}_\delta^{\text{lin}}(k) = \mathcal{P}_\zeta(k) T^2(k). \quad (7)$$

Note that, when calculating Eq. (6), we make the approximation $\mathcal{P}_\zeta^{\text{add}}(k) = \mathcal{A}_\zeta^{\text{add}} \delta(\ln(k) - \ln(k_{\text{sp}}))$, for simplicity and employ the pointwise window function for \tilde{W}_k following the BBKS. Then the mass of the formed EFHs is limited to only $M_h(k_{\text{sp}})$ calculated in Eq. (3).

III. LENSING POTENTIAL WITH EFHS

In order to discuss the effect of EFHs on the CMB anisotropy, we focus on the CMB anisotropy power spectra for temperature (C_ℓ^{TT}), E-mode (C_ℓ^{EE}), and B-mode polarization (C_ℓ^{BB}). These lensed CMB observables can

be calculated through [43]

$$\begin{aligned} C_\ell^{\text{L},TT} & \approx (1 - \ell^2 R^\phi) C_\ell^{\text{TT}} \\ & + \int \frac{d^2 \ell'}{(2\pi)^2} [\ell' \cdot (\ell - \ell')]^2 C_{|\ell - \ell'|}^{\phi\phi} C_{\ell'}^{\text{TT}}, \\ C_\ell^{\text{L},EE} & \approx (1 - \ell^2 R^\phi) C_\ell^{\text{EE}} \\ & + \int \frac{d^2 \ell'}{(2\pi)^2} [\ell' \cdot (\ell - \ell')]^2 C_{|\ell - \ell'|}^{\phi\phi} C_{|\ell'|}^{\text{EE}} \cos^2 2(\phi_{\ell'} - \phi_\ell), \\ C_\ell^{\text{L},BB} & \approx \int \frac{d^2 \ell'}{(2\pi)^2} [\ell' \cdot (\ell - \ell')]^2 C_{|\ell - \ell'|}^{\phi\phi} C_{|\ell'|}^{\text{EE}} \sin^2 2(\phi_{\ell'} - \phi_\ell), \end{aligned} \quad (8)$$

where the superscript L denotes the lensed field and R^ϕ is half of a total deflection angle power,

$$R^\phi \equiv \frac{1}{2} \langle |\nabla \phi|^2 \rangle = \frac{1}{4\pi} \int \frac{d\ell}{\ell} \ell^4 C_\ell^{\phi\phi}. \quad (9)$$

Note that we neglect the primordial B-mode polarization. This would be justified by the current observational status so that the source of the primordial B-mode polarization is severely restricted, *e.g.*, in the term of the tensor-to-scalar ratio r , $r < 0.036$ [44].

In Equation (8), $C_\ell^{\phi\phi}$ is the angular power spectrum of the lensing potential, which is defined by

$$\phi(\hat{n}) \equiv -2 \int_0^{\chi_s} d\chi \frac{\chi_s - \chi}{\chi s \chi} \Phi(\chi \hat{n}; \eta_0 - \chi), \quad (10)$$

where χ represents the comoving distance and χ_s is the comoving distance to a source, *i.e.*, the last scattering surface in this work.

Accordingly, the angular power spectrum of the lensing potential can be calculated by [43]

$$\begin{aligned} C_\ell^{\phi\phi} & = 16\pi \int \frac{dk}{k} \int_0^{\chi_s} d\chi \int_0^{\chi_s} d\chi' \mathcal{P}_\Phi(k; \eta_0 - \chi, \eta_0 - \chi') \\ & \quad \times j_\ell(k\chi) j_\ell(k\chi') \left(\frac{\chi_s - \chi}{\chi s \chi} \right) \left(\frac{\chi_s - \chi'}{\chi s \chi'} \right) \\ & \approx 16\pi \int \frac{dk}{k} \int_0^{\chi_s} d\chi \mathcal{P}_\Phi(k; \eta_0 - \chi) \left(\frac{\chi_s - \chi}{\chi s \chi} \right)^2, \end{aligned} \quad (11)$$

where $\mathcal{P}_\Phi(k; \eta, \eta')$ is a dimensionless power spectrum of the gravitational potential Φ at η and η' which is defined as

$$\langle \tilde{\Phi}(\mathbf{k}; \eta) \tilde{\Phi}^*(\mathbf{k}'; \eta') \rangle = \frac{2\pi^2}{k^3} \mathcal{P}_\Phi(k; \eta, \eta') \delta(\mathbf{k} - \mathbf{k}'), \quad (12)$$

and $\mathcal{P}_\Phi(k; \eta) \equiv \mathcal{P}_\Phi(k; \eta, \eta)$. To obtain the last equation in Eq. (11), we apply the Limber approximation because in the calculation of the lensed CMB anisotropy, the main contribution comes from the angular power spectrum of the lensing potential on small scales $\ell \gtrsim 100$.

Using the Poisson equation, \mathcal{P}_Φ is related to a dimensionless matter power spectrum \mathcal{P}_δ as

$$\mathcal{P}_\Phi(k; \eta) = \frac{9}{4} \Omega_m^2(\eta) \mathcal{H}^4(\eta) \frac{\mathcal{P}_\delta(k; \eta)}{k^4}, \quad (13)$$

where $\mathcal{H}(\eta)$ is the conformal Hubble parameter in respect to η . One can find that the angular power spectrum of the lensing potential depends on the matter power spectrum $\mathcal{P}_\delta(k; \eta)$ through Eqs. (11) and (13).

In the calculation of the CMB lensing, the effect of the nonlinear structure, like DM halos, is not negligible. Therefore, it is required to obtain the nonlinear matter power spectrum instead of the linear one as shown in Eq. (7) for a calculation of Eq. (13). Similarly to the primordial perturbations as in Eq. (1), we can classify the nonlinear matter power spectrum into two parts as

$$\mathcal{P}_\delta = \mathcal{P}_\delta^{\text{st}}(k; \eta) + \mathcal{P}_\delta^{\text{add}}(k; \eta). \quad (14)$$

Here, while $\mathcal{P}_\delta^{\text{st}}(k; \eta)$ is the contribution to the matter power spectrum from the the standard almost-scale-invariant power spectrum, $\mathcal{P}_\delta^{\text{add}}(k; \eta)$ is the one from the spike-type power spectrum.

Though many references have studied such nonlinear effects due to the almost-scale-invariant power spectrum accurately, we employ the `HMCode` presented in Ref. [45] for the calculation of $\mathcal{P}_\delta^{\text{st}}(k; \eta)$, including the nonlinear effects.

To obtain $\mathcal{P}_\delta^{\text{add}}(k; \eta)$, it is necessary to consider the spike-type primordial power spectrum and the nonlinear effects induced by EFHs. Following Ref. [46], the dimensionless matter power spectrum with the nonlinear effect can be written by

$$\mathcal{P}_\delta^{\text{add}}(k; \eta) = \mathcal{P}_\delta^{\text{hh}}(k; \eta) + \mathcal{P}_\delta^{\text{P}}(k; \eta), \quad (15)$$

where $\mathcal{P}_\delta^{\text{P}}$ is the Poisson term, and $\mathcal{P}_\delta^{\text{hh}}$ is the halo-halo correlation term.

In the case of EFHs, we obtain both terms using Eq. (4) as

$$\mathcal{P}_\delta^{\text{P}}(k; \eta) = \frac{k^3}{2\pi^2} \frac{n(\eta) M_h^2}{\bar{\rho}_m^2} |\tilde{y}[k, M_h]|^2, \quad (16)$$

and

$$\mathcal{P}_\delta^{\text{hh}}(k; \eta) = D_+^2(\eta) \mathcal{P}_\delta^{\text{lin}}(k) \left[\frac{n(\eta) M_h}{\bar{\rho}_m} b_h \tilde{y}[k, M_h] \right]^2, \quad (17)$$

where $\mathcal{P}_\delta^{\text{lin}}(k)$ is the present linear matter power spectrum given in Eq. (7), b_h is a bias factor for EFHs based on the peak theory [47], and \tilde{y} is a Fourier function of the density profile inside EFHs normalized by M_h .

For the density profile of EFHs, we adopt the Navarro-Frenk-White (NFW) profile,

$$\rho(r) = \frac{\rho_s}{(r/r_s)(1+r/r_s)^2}, \quad (18)$$

where ρ_s is the characteristic density and r_s is the scale radius. The scale radius relates to the concentration parameter, $c = r_{\text{vir}}/r_s$ with a virial radius r_{vir} . This concentration parameter generally depends on the mass and redshift, often referred to as the mass-concentration parameter relation. In this work, we adopt a fitting formula presented by Ref. [48] and updated parameters of mass-concentration relation [49, 50].

It is worth mentioning that there are some arguments and suggestions about the several density profiles for the EFHs, which are different from the NFW profile, based on the radial infall similarity solution [51] and numerical simulations [24, 25, 52]. However, since the density profile dependence arises below the scales of the EFH radius in the CMB lensing anisotropy, the choice of the density profile does not affect our results in our interesting scales, $\ell \lesssim \mathcal{O}(10^4)$.

We calculate and plot the matter power spectrum with the additional spike-type power spectrum at $z = 10$ in Fig. 2. In the calculation, we include the nonlinear effects of EFHs, as discussed above. The blue solid line is for a parameter set of $(k_{\text{sp}}[\text{Mpc}^{-1}], \mathcal{A}_\zeta) = (3.4, 10^{-6})$ and the orange solid line is for $(k_{\text{sp}}[\text{Mpc}^{-1}], \mathcal{A}_\zeta) = (16.0, 10^{-7})$. The dash-dot and the dashed lines represent the Poisson term and the halo-halo correlation term of EFHs, respectively. For comparison, we represent the nonlinear standard matter power spectrum, $\mathcal{P}_\delta^{\text{st}}(k; \eta)$, in the black solid line.

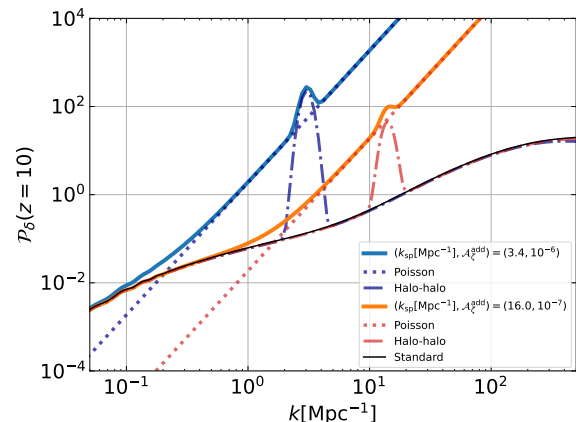


FIG. 2. Matter power spectrum including the additional spike-type power and nonlinear effects of EFHs at $z = 10$ with two parameter sets of $(k_{\text{sp}}[\text{Mpc}^{-1}], \mathcal{A}_\zeta^{\text{add}}) = (3.4, 10^{-6})$ (blue) and $(16.0, 10^{-7})$ (orange). The dash-dot and the dashed lines represent the Poisson term and the halo-halo correlation term of EFHs, respectively. For comparison, we also represent the nonlinear standard matter power spectrum, $\mathcal{P}_\delta^{\text{st}}(k; \eta)$, in the black solid line.

EFHs form earlier than the standard hierarchical structure generated from the scale-invariant spectrum $\mathcal{P}_\zeta^{\text{st}}(k)$. However as the universe evolves, $\mathcal{P}_\zeta^{\text{st}}(k)$ can produce more massive DM halos than EFHs. In the formation

of such massive halos, most of the EFHs would be captured into them. After being captured, EFHs become subhalos or are destroyed by tidal disruption, and so on. As a result, $\mathcal{P}_\delta^{\text{add}}$ describing the nonlinear effect due to EFHs can be subdominant compared with $\mathcal{P}_\delta^{\text{st}}$ in the late universe. To take the effect into account, we introduce z_{suv} as the typical redshift in which EFHs are captured into massive halos in the standard hierarchical structure formation. We assume that, since EFHs cannot survive as isolated objects after z_{suv} , we neglect the nonlinear effects of EFHs in \mathcal{P}_δ after z_{suv} . We will discuss the value of z_{suv} later.

Figure 3 shows the angular power spectrum of lensing potential. The black solid line shows the standard one, including nonlinear effects from standard DM halos. In contrast, the black dotted line depicts the standard linear spectrum. The colour solid lines represent the lensed angular power spectrum, including the nonlinear effect with EFHs and standard DM halos, while the colour dotted lines depict the linear spectrum, including only the additional primordial power spectrum in Eq. (2). The same manner of colour in Figs. 1 and 2 is adopted. Here, when calculating the solid lines, we fix the value of z_{suv} based on the redshift at which the standard hierarchical structure formation, possessing a mass of $M = 10^{12}M_\odot$ and $M = 10^{10}M_\odot$, becomes efficient, respectively; we set z_{suv} as $\delta_c/\sigma(M, z_{\text{suv}}) = 1$, where σ is the mass variance calculated from the standard matter power spectrum. For instance, we adopt $z_{\text{suv}} \approx 2$ for the blue line, and $z_{\text{suv}} \approx 4$ for the orange line. We also plot the observation data by SPTpol [53] in red for comparison.

In Figure 3, we find the nonlinear effects through EFHs and standard halos give non-negligible enhancement in addition to the large bump induced by the spike-type enhancement in Eq. (2). We also put an enlarged figure of the $C_\ell^{\phi\phi}$ s around $\ell = 1000$. Since the spectrum of $C_\ell^{\phi\phi}$ with different models matches on large scales, $\ell < 1000$, their magnitude relationship around $\ell = 1000$ decides the one of the total deflection angle power in Eq. (9).

IV. RESULTS & DISCUSSION

In order to calculate the lensed CMB anisotropy with the EFH effects, we employ the public Boltzmann code, CAMB [42]. We modified CAMB [42] to include the spike enhancement in the primordial power spectrum represented in Eq. (2) and the nonlinear effects by the existence of EFHs expressed in Eqs. (16) and (17). Also, as we mentioned before, we employ analytical formulae of HMCODE [45] to calculate the nonlinear matter power spectrum with the standard structure formation scenario.

The left panel of Fig. 4 shows the results of the lensed CMB temperature anisotropy with the EFH effect. In the upper part, the vertical axis shows \mathcal{D}_ℓ^{TT} in unit of μK^2 , where $\mathcal{D}_\ell^{XX} \equiv \ell(\ell + 1)C_\ell^{XX}$. The blue lines show the anisotropies related to the model of ($k_{\text{sp}} = 3.4\text{Mpc}^{-1}, \mathcal{A}_\ell^{\text{add}} = 10^{-6}$), while the black lines show the

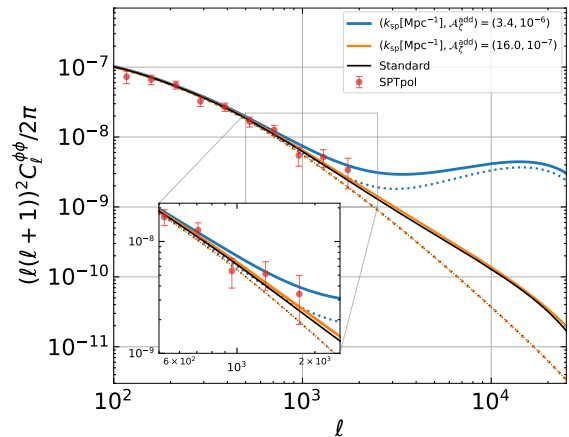


FIG. 3. The angular power spectrum of lensing potentials including EFHs. The black solid line shows the standard one, including nonlinear effects from standard DM halos, while the black dotted line depicts the standard linear spectrum. The colour solid lines represent the lensed angular power spectrum, including the nonlinear effect with EFHs and standard DM halos. The colour dotted lines depict the linear spectrum, including only the additional primordial power spectrum in Eq. (2). The same manner of colour in Figs. 1 and 2 is adopted. For reference, we also plot the observation data by SPTpol [53] (red) with $\pm 1\sigma$ error bar.

standard anisotropies. The black (blue) solid lines depict the lensed anisotropies, including nonlinear effects from standard halos (and EFHs). For the comparison, we also plot the linear lensed anisotropies for the primordial power spectrum in Eq. (1) in the blue dotted line and the unlensed anisotropies in dashed lines. In addition, we plot the observation data by SPT-SZ [54] for reference. In the lower part, we plot the ratio of the blue and black solid lines against the blue dotted line.

The lensing effect enhances the amplitude of the anisotropy on small scales. We find that the lensed anisotropy with the nonlinear effects of EFHs and standard DM halos, *i.e.*, the blue solid line, is comparable to or larger than the thermal SZ effect by galaxy clusters or other sources, including dusty, star-forming, and radio galaxies, although it does not reach the level of the observed signal. These signals have different frequency dependencies, while our lensed CMB anisotropy is independent of the frequency. Component decomposition through multi-frequency observations would provide more stringent constraints on our lensed signal and, subsequently, on the abundance of the EFH and the feature of the spike-type power spectrum.

We also calculate the lensed anisotropy of the CMB polarization. The middle panel of Fig. 4 shows the lensed anisotropy of the CMB E-mode polarization $\mathcal{D}_\ell^{L,EE}$. The plotting manner is the same as in the left panel of Fig. 4. We also plot the observation data by SPTpol [55] for comparison. Similarly to the temperature anisotropy, the

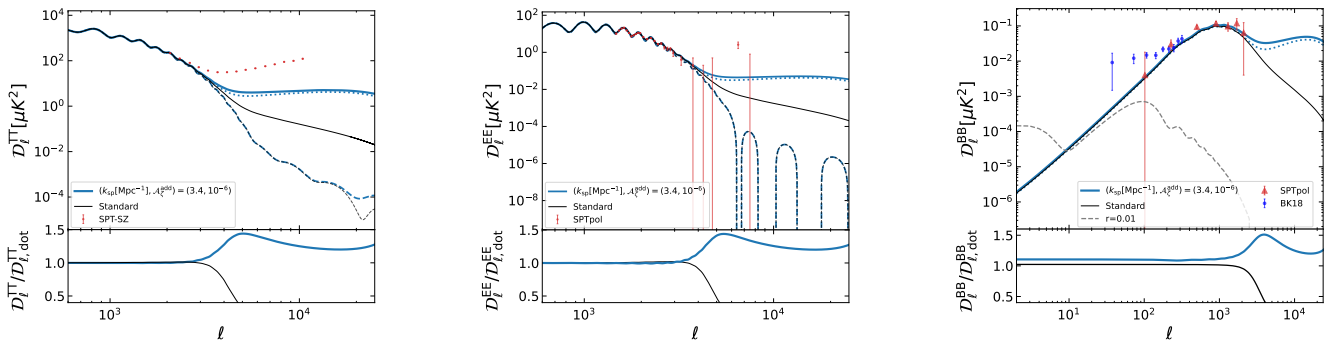


FIG. 4. The lensed CMB angular power spectrum. The upper panel shows the angular power spectrum with respect to D_ℓ in the unit of $(\mu\text{K})^2$. The black line shows the spectrum with standard DM halos, and the coloured line depicts the one with EFHs and standard DM halos. The solid line shows the spectrum, including the nonlinear effect with EFHs or/and standard DM halos, while the dotted line represents the linear spectrum. The dashed line represents the unlensed spectrum. The lower panel represents the ratio of the blue and black solid lines against the blue dotted line. For reference, we also plot the observation data by SPT-SZ [54], SPTpol [53, 55] and BICEP/KECK [44] with $\pm 1\sigma$ error bars. *Left*: CMB temperature, *Middle*: CMB E-mode polarization, *Right*: CMB B-mode polarization.

lensing effect of the EFHs arises on small scales as the enhancement of the anisotropy signals. According to the current observation data of the E-mode polarization, it is difficult to provide the constraint on the abundance of the EFHs due to the large error bars of the E-mode polarization measurement. However, the figure suggests that the improvement of the observation measurement, for example, the decreasing the error to 10 % level of the current level, could provide the limit on the EFH abundance and the spike-type power spectrum of $(k_{\text{sp}} = 3.4\text{Mpc}^{-1}, \mathcal{A}_\zeta^{\text{add}} = 10^{-6})$.

The right panel of Fig. 4 represents the lensed anisotropy of the CMB B-mode polarization $D_\ell^{L,BB}$ with the same manner as in the left and middle panels. Additionally, we plot the observation data by SPTpol [53] and BICEP/KECK [44] in red and blue points, respectively. As mentioned before, we calculate the lensed anisotropies, assuming that the primordial (unlensed) anisotropy of B-mode polarization can be negligible. However, we here plot the primordial B-mode polarization anisotropy with the tensor-to-scalar ratio of $r = 0.01$ in the black dotted line for comparison.

In the B-mode polarization, the enhancement due to the EFHs arises on small scales, as in the temperature and E-mode polarization. Since there are no sources of B-mode polarization other than the gravitational lensing in our calculation, the enhancement leads to the significant feature of the B-mode polarization on small scales.

Besides, the lensed B-mode signals are calculated by integrating $C_\ell^{\phi\phi}$ overall range of ℓ -modes. Therefore, although the existence of the EFHs amplify $C_\ell^{\phi\phi}$ on small scales, this amplification affects all range of ℓ modes in the lensed B-mode through the integration. As a result, the EFH effect on the B-mode polarization appears even on large scales as the overall enhancement by 10 % level.

Note that degeneracy between the flat enhancement

and the amplitude of the standard primordial power spectrum \mathcal{A}_ζ can break using, *e.g.*, CMB temperature and E-mode polarization anisotropies on scales of $\ell \leq 10^3$. Actually in the Planck analysis, the value of \mathcal{A}_ζ is obtained in the $\sim 5\%$ accuracy, $\mathcal{A}_\zeta = 2.1_{-0.1}^{+0.1} \times 10^{-9}$. While current CMB polarization measurements on large scales are constrained by instrumental noise, forthcoming projects such as CLASS [56], Groundbird [57], and PIPER [58], can address the B-mode polarization anisotropies accurately, with limitations primarily imposed by the cosmic variance. Notably, the LiteBIRD satellite [59] planned to be launched in the late 2020s will conduct polarimetric observations across the entire sky, employing fifteen frequency bands to address the foreground predicament. Therefore, though the principal objective of these experiments is to detect the primordial B-mode anisotropy, our model can be testable through these future experiments.

Lastly, we mention the results of adapting the parameter set of $(k_{\text{sp}}[\text{Mpc}^{-1}], \mathcal{A}_\zeta) = (16.0, 10^{-7})$ to see the dependence of C_ℓ^L on our models, which is plotted in Fig. 5. In the upper panels of Fig. 5, the plotting manner is the same as in the ones of Fig. 4. The orange lines show the spectrum with the parameter set of $(k_{\text{sp}}[\text{Mpc}^{-1}], \mathcal{A}_\zeta) = (16.0, 10^{-7})$. In the lower panel, we show the ratio of the blue and orange solid lines against the black solid line. As in the case of parameter set of $(k_{\text{sp}}[\text{Mpc}^{-1}], \mathcal{A}_\zeta) = (3.4, 10^{-6})$, the nonlinear effects of EFHs and the presence of a spike-type primordial power spectrum lead to a change in the lensed anisotropy. However, as expected from Fig. 3, the magnitude of the enhancement is too small to detect mainly because of the peak location of the additional spike-type primordial power spectrum (see Appendix A for the dependency on the peak amplitude). Combining the dependency of $(\ell(\ell+1))^2 C_\ell^{\phi\phi} \propto \ell^{-2}$ and Eq. (8), one can find that the enhancement of $C_\ell^{\phi\phi}$ on small scales, $\ell > 10^4$, no longer

affects the lensed CMB anisotropies. Actually, in this case of $k_{\text{sp}} = 3.4 \text{Mpc}^{-1}$, we confirm that setting higher amplitude of \mathcal{A}_ζ does not change the result. Hence, we find that the accurate measurements of the anisotropy of lensing potentials and the lensed CMB anisotropy would provide insight into the abundance of EFHs with the mass of $\sim 10^{12} M_\odot$ and the primordial power spectrum on the limited scales around $k \sim 1 \text{Mpc}^{-1}$.

V. CONCLUSION

Some theoretical models for the early universe, including the inflationary expansion scenario, predict a spike-type enhancement in the primordial power spectrum on small scales. Such enhanced fluctuations form EFHs, which could significantly impact the structure formation and cosmological signals. In this study, we have studied the CMB gravitational lensing effect, considering the existence of the spike-type primordial power spectrum and the nonlinear effects of EFHs, and investigated the potential to probe the EFHs and their origin, *i.e.*, primordial perturbations on scales smaller than 1 Mpc.

This work has investigated two different spike-type power spectra with $(k_{\text{sp}}[\text{Mpc}^{-1}], \mathcal{A}_\zeta^{\text{add}}) = (3.4, 10^{-6})$ and $(16.0, 10^{-7})$ as examples. We have numerically calculated the CMB observables, such as the angular power spectrum of the lensing potential and the lensed CMB anisotropy of temperature, E-mode, and B-mode polarization for the two power spectra using the modified **CAMB**. We have found that the effect of the spike-type power spectrum and EFHs on the CMB observables arises on small scales, as shown in Figs. 3, 4 and 5. Regarding the lensed anisotropies of the CMB temperature and E-mode polarization with $(k_{\text{sp}}[\text{Mpc}^{-1}], \mathcal{A}_\zeta^{\text{add}}) = (3.4, 10^{-6})$, we have found the possibility that the signals are significantly enhanced and could be discussed by component decomposition of observed signals through multi-frequency observations or improvements of the measurements. As for the lensed anisotropy of CMB B-mode polarization, we have found that the effect of the spike-type power spectrum and EFHs appears even on large scales, $\ell < 100$, as the overall enhancement by $\sim 10\%$ level compared to the standard one. Although the current CMB observation does not have the sensitivity to distinguish 10% difference on the scales, the future measurements on CMB B-mode polarization on large scales, such as the LiteBIRD satellite, have the potential to test

the existence of EFHs and the spike-type power spectrum on small scales.

On the other hand, we have found that the enhancement by the effect of the spike-type power spectrum and EFHs with $(k_{\text{sp}}[\text{Mpc}^{-1}], \mathcal{A}_\zeta^{\text{add}}) = (16.0, 10^{-7})$ is too small to detect both because of the amplitude and peak location of the additional spike-type primordial power spectrum. Therefore, we have found that the accurate measurements of the CMB lensing effect would provide insight into the abundance of EFHs within the limited mass range around $10^{12} M_\odot$ and the primordial power spectrum on the limited scales around $k \sim 1 \text{Mpc}^{-1}$.

ACKNOWLEDGMENTS

We thank V. Nistane for the useful discussions and for the cooperation in developing the modified **CAMB** code. This work was supported by JSPS KAKENHI Grant Numbers 21K03533.

Appendix A: $\mathcal{A}_\zeta^{\text{add}}$ dependency

We show dependencies of $C_\ell^{\phi\phi}$ and the lensed CMB angular power spectrum such as $C_\ell^{L,TT}$, $C_\ell^{L,EE}$, and $C_\ell^{L,BB}$ on $\mathcal{A}_\zeta^{\text{add}}$. We calculate for three models, $\mathcal{A}_\zeta^{\text{add}} = 10^{-5}$, 10^{-6} , and 10^{-7} . Although the model of $\mathcal{A}_\zeta^{\text{add}} = 10^{-5}$ would already be excluded through the measurement of CMB spectral distortions by COBE/FIRAS, we show as the example. Here, we fix the value of k_{sp} as $k_{\text{sp}} = 3.4 \text{Mpc}^{-1}$. Figure 6 shows the dependencies. The upper left panel shows $C_\ell^{\phi\phi}$ represented by the dark blue line for the model of $\mathcal{A}_\zeta^{\text{add}} = 10^{-5}$, the blue line for $\mathcal{A}_\zeta^{\text{add}} = 10^{-6}$, and the light blue for $\mathcal{A}_\zeta^{\text{add}} = 10^{-7}$. The black solid and dotted lines show the standard angular power spectrum with and without lensing effects. We can find that the model of $\mathcal{A}_\zeta^{\text{add}} = 10^{-5}$ would also be constrained through the measurement of $C_\ell^{\phi\phi}$. The upper right panel shows $C_\ell^{L,TT}$, which is plotted in the same manner as the panel of $C_\ell^{\phi\phi}$. While the lower left panel shows $C_\ell^{L,EE}$, the lower right panel shows $C_\ell^{L,BB}$. We find at most *sim*25% increments of the amplitude of the CMB B-mode polarization anisotropy with the model of $\mathcal{A}_\zeta^{\text{add}} = 10^{-5}$ on large scales, while the enhancement with the model of $\mathcal{A}_\zeta^{\text{add}} = 10^{-7}$ is too small to detect.

-
- [1] Planck Collaboration and N. e. a. Aghanim, Planck 2018 results. VI. Cosmological parameters, ArXiv e-prints (2018), [arXiv:1807.06209](https://arxiv.org/abs/1807.06209).
- [2] P. McDonald, U. Seljak, S. Burles, D. J. Schlegel, D. H. Weinberg, R. Cen, D. Shih, J. Schaye, D. P. Schneider, N. A. Bahcall, J. W. Briggs, J. Brinkmann, R. J. Brun-

- ner, M. Fukugita, J. E. Gunn, Ž. Ivezić, S. Kent, R. H. Lupton, and D. E. Vanden Berk, The Ly α Forest Power Spectrum from the Sloan Digital Sky Survey, *ApJS* **163**, 80 (2006), [arXiv:astro-ph/0405013](https://arxiv.org/abs/astro-ph/0405013) [astro-ph].
- [3] S. Chabanier, N. Palanque-Delabrouille, C. Yèche, J.-M. Le Goff, E. Armengaud, J. Bautista, M. Blomqvist,

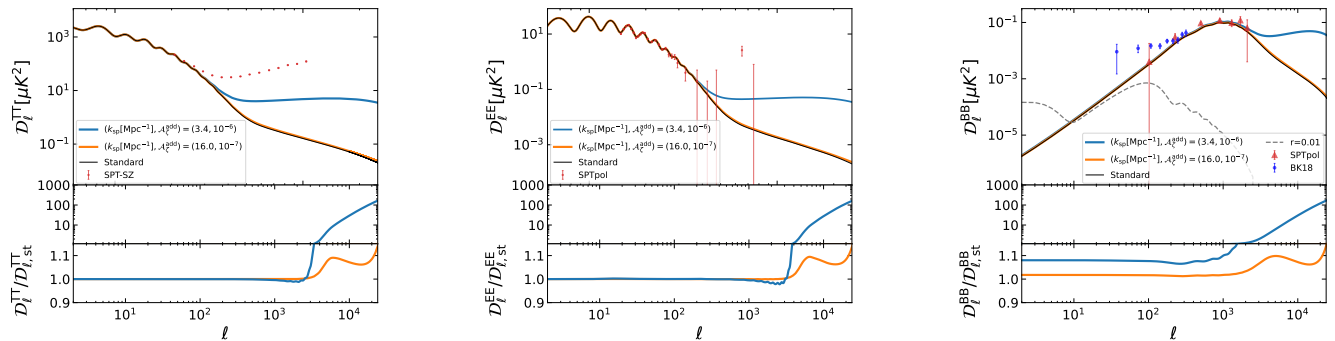


FIG. 5. The lensed CMB angular power spectrum. In the upper panel, the plotting manner is the same as in Fig. 4. The orange lines show the spectrum with the parameter set of $(k_{\text{sp}}[\text{Mpc}^{-1}], \mathcal{A}_s) = (16.0, 10^{-7})$. In the lower panel, we show the ratio of the blue and orange solid lines against the black solid line. *Left*: CMB temperature, *Middle*: CMB E-mode polarization, *Right*: CMB B-mode polarization.

- N. Busca, K. Dawson, T. Etourneau, A. Font-Ribera, Y. Lee, H. du Mas des Bourboux, M. Pieri, J. Rich, G. Rossi, D. Schneider, and A. Slosar, The one-dimensional power spectrum from the SDSS DR14 Ly α forests, *J. Cosmology Astropart. Phys.* **2019**, 017 (2019), [arXiv:1812.03554](https://arxiv.org/abs/1812.03554) [astro-ph.CO].
- [4] B. Joachimi, C. A. Lin, M. Asgari, T. Tröster, C. Heymans, H. Hildebrandt, F. Köhlinger, A. G. Sánchez, A. H. Wright, M. Bilicki, C. Blake, J. L. van den Busch, M. Crocce, A. Dvornik, T. Erben, F. Getman, B. Giblin, H. Hoekstra, A. Kannawadi, K. Kuijken, N. R. Napolitano, P. Schneider, R. Scoccimarro, E. Sclentini, H. Y. Shan, M. von Wietersheim-Kramsta, and J. Zuntz, KiDS-1000 methodology: Modelling and inference for joint weak gravitational lensing and spectroscopic galaxy clustering analysis, *A&A* **646**, A129 (2021), [arXiv:2007.01844](https://arxiv.org/abs/2007.01844) [astro-ph.CO].
- [5] M. Costanzi, A. Saro, S. Bocquet, T. M. C. Abbott, M. Aguena, S. Allam, A. Amara, J. Annis, S. Avila, D. Bacon, B. A. Benson, S. Bhargava, D. Brooks, E. Buckley-Geer, D. L. Burke, A. Carnero Rosell, M. Carrasco Kind, J. Carretero, A. Choi, L. N. da Costa, M. E. S. Pereira, J. De Vicente, S. Desai, H. T. Diehl, J. P. Dietrich, P. Doel, T. F. Eifler, S. Everett, I. Ferrero, A. Ferté, B. Flaugher, P. Fosalba, J. Frieman, J. García-Bellido, E. Gaztanaga, D. W. Gerdes, T. Giannantonio, P. Giles, S. Grandis, D. Gruen, R. A. Gruendl, N. Gupta, G. Gutierrez, W. G. Hartley, S. R. Hinton, D. L. Hollowood, K. Honscheid, D. J. James, T. Jeltema, E. Krause, K. Kuehn, N. Kuropatkin, O. Lahav, M. Lima, N. MacCrann, M. A. G. Maia, J. L. Marshall, F. Menanteau, R. Miquel, J. J. Mohr, R. Morgan, J. Myles, R. L. C. Ogando, A. Palmese, F. Paz-Chinchón, A. A. Plazas, D. Rapetti, C. L. Reichardt, A. K. Romer, A. Roodman, F. Ruppin, L. Salvati, S. Samuroff, E. Sanchez, V. Scarpine, S. Serrano, I. Sevilla-Noarbe, P. Singh, M. Smith, M. Soares-Santos, A. A. Stark, E. Suchyta, M. E. C. Swanson, G. Tarle, D. Thomas, C. To, D. L. Tucker, T. N. Varga, R. H. Wechsler, Z. Zhang, DES, and SPT Collaborations, Cosmological constraints from DES Y1 cluster abundances and SPT multiwavelength data, *Phys. Rev. D* **103**, 043522 (2021), [arXiv:2010.13800](https://arxiv.org/abs/2010.13800) [astro-ph.CO].
- [6] M. Hilton, C. Sifón, S. Naess, M. Madhavacheril, M. Oguri, E. Rozo, E. Rykoff, T. M. C. Abbott, S. Adhikari, M. Aguena, S. Aiola, S. Allam, S. Amodeo, A. Amon, J. Annis, B. Ansarinejad, C. Aros-Bunster, J. E. Austermann, S. Avila, D. Bacon, N. Battaglia, J. A. Beall, D. T. Becker, G. M. Bernstein, E. Bertin, T. Bhandarkar, S. Bhargava, J. R. Bond, D. Brooks, D. L. Burke, E. Calabrese, M. Carrasco Kind, J. Carretero, S. K. Choi, A. Choi, C. Conselice, L. N. da Costa, M. V. Costanzi, D. Crichton, K. T. Crowley, R. Dünner, E. V. Denison, M. J. Devlin, S. R. Dicker, H. T. Diehl, J. P. Dietrich, P. Doel, S. M. Duff, A. J. Duivenvoorden, J. Dunkley, S. Everett, S. Ferraro, I. Ferrero, A. Ferté, B. Flaugher, J. Frieman, P. A. Gallardo, J. García-Bellido, E. Gaztanaga, D. W. Gerdes, P. Giles, J. E. Golec, M. B. Gralla, S. Grandis, D. Gruen, R. A. Gruendl, J. Gschwend, G. Gutierrez, D. Han, W. G. Hartley, M. Hasselfield, J. C. Hill, G. C. Hilton, A. D. Hincks, S. R. Hinton, S. P. P. Ho, K. Honscheid, B. Hoyle, J. Hubmayr, K. M. Huffenberger, J. P. Hughes, A. T. Jaelani, B. Jain, D. J. James, T. Jeltema, S. Kent, K. Knowles, B. J. Koopman, K. Kuehn, O. Lahav, M. Lima, Y. T. Lin, M. Lokken, S. I. Loubser, N. MacCrann, M. A. G. Maia, T. A. Marriage, J. Martin, J. McMahon, P. Melchior, F. Menanteau, R. Miquel, H. Miyatake, K. Moodley, R. Morgan, T. Mroczkowski, F. Nati, L. B. Newburgh, M. D. Niemack, A. J. Nishizawa, R. L. C. Ogando, J. Orłowski-Scherer, L. A. Page, A. Palmese, B. Partridge, F. Paz-Chinchón, P. Phakathi, A. A. Plazas, N. C. Robertson, A. K. Romer, A. Carnero Rosell, M. Salatino, E. Sanchez, E. Schaan, A. Schillaci, N. Sehgal, S. Serrano, T. Shin, S. M. Simon, M. Smith, M. Soares-Santos, D. N. Spergel, S. T. Staggs, E. R. Storer, E. Suchyta, M. E. C. Swanson, G. Tarle, D. Thomas, C. To, H. Trac, J. N. Ullom, L. R. Vale, J. Van Lanen, E. M. Vavagiakis, J. De Vicente, R. D. Wilkinson, E. J. Wollack, Z. Xu, and Y. Zhang, The Atacama Cosmology Telescope: A Catalog of $\gtrsim 4000$ Sunyaev-Zel'dovich Galaxy Clusters, *ApJS* **253**, 3 (2021), [arXiv:2009.11043](https://arxiv.org/abs/2009.11043) [astro-ph.CO].
- [7] DES Collaboration, T. M. C. Abbott, M. Aguena, A. Alarcon, S. Allam, O. Alves, A. Amon, F. Andrade-Oliveira, J. Annis, S. Avila, D. Bacon, E. Baxter, K. Bechtol, M. R. Becker, G. M. Bernstein, S. Bhar-

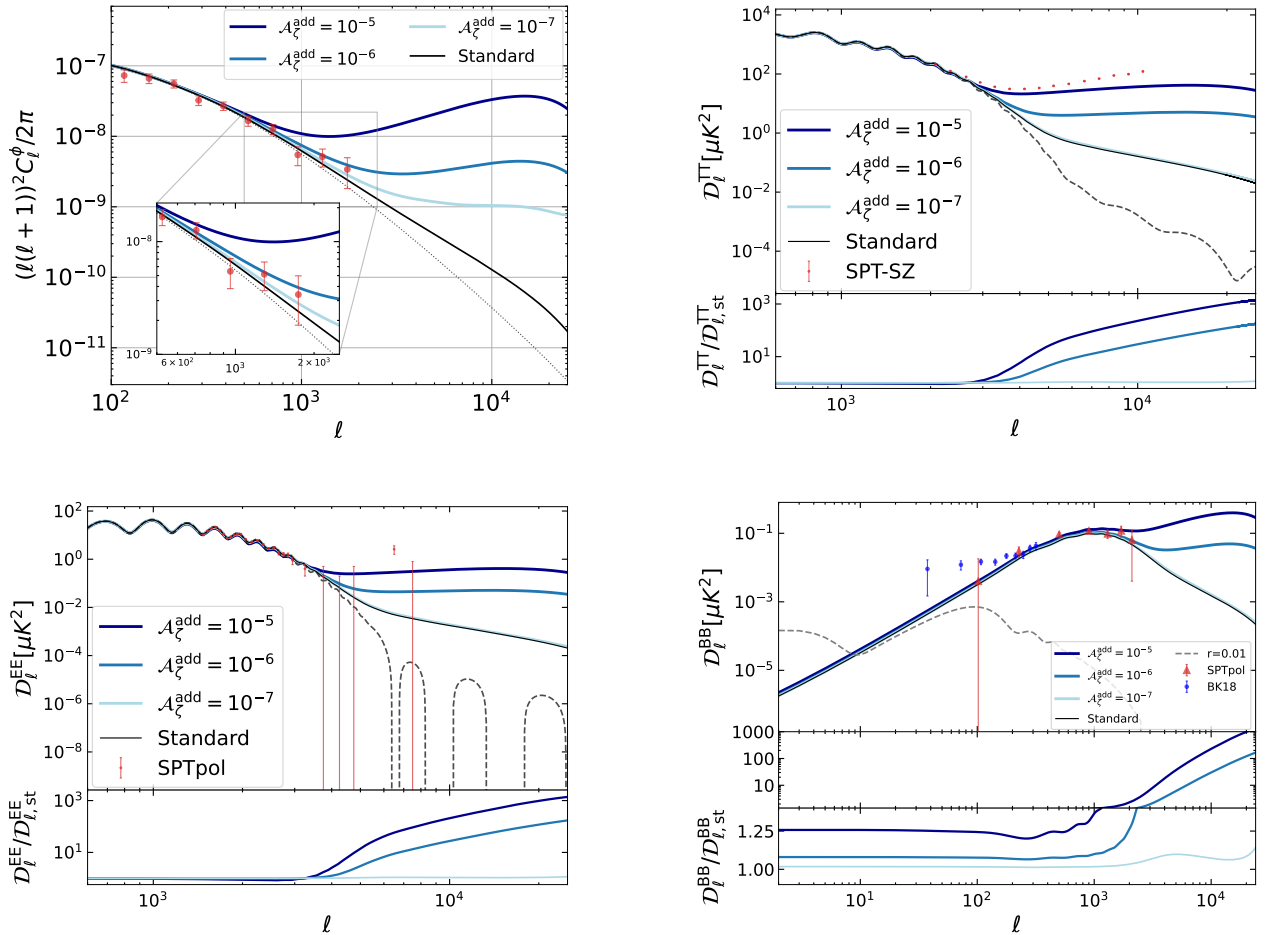


FIG. 6. The angular power spectrum of the lensing potential and the lensed angular power spectrum of the CMB temperature, E-mode, and B-mode polarization with three models, $\mathcal{A}_\zeta^{\text{add}} = 10^{-5}$ (dark blue), 10^{-6} (blue), and 10^{-7} (light blue). We fix the value of k_{SP} , $k_{\text{SP}} = 3.4 \text{Mpc}^{-1}$. *Upper left*: The angular power spectrum of the lensing potential, *Upper right*: The lensed angular power spectrum of the CMB temperature, *Lower left*: The lensed angular power spectrum of the CMB E-mode polarization, *Lower right*: The lensed angular power spectrum of the CMB B-mode polarization.

gava, S. Birrer, J. Blazek, A. Brandao-Souza, S. L. Bridle, D. Brooks, E. Buckley-Geer, D. L. Burke, H. Camacho, A. Campos, A. Carnero Rosell, M. Carrasco Kind, J. Carretero, F. J. Castander, R. Cawthon, C. Chang, A. Chen, R. Chen, A. Choi, C. Conselice, J. Cordero, M. Costanzi, M. Crocce, L. N. da Costa, M. E. da Silva Pereira, C. Davis, T. M. Davis, J. De Vicente, J. DeRose, S. Desai, E. Di Valentino, H. T. Diehl, J. P. Dietrich, S. Dodelson, P. Doel, C. Doux, A. Drlica-Wagner, K. Eckert, T. F. Eifler, F. Elsner, J. Elvin-Poole, S. Everett, A. E. Evrard, X. Fang, A. Farahi, E. Fernandez, I. Ferrero, A. Ferté, P. Fosalba, O. Friedrich, J. Frieman, J. García-Bellido, M. Gatti, E. Gaztanaga, D. W. Gerdes, T. Giannantonio, G. Giannini, D. Gruen, R. A. Gruendl, J. Gschwend, G. Gutierrez, I. Harrison, W. G. Hartley, K. Herner, S. R. Hinton, D. L. Hollowood, K. Honscheid, B. Hoyle, E. M. Huff, D. Huterer, B. Jain, D. J. James, M. Jarvis, N. Jeffrey, T. Jeltema, A. Kovacs, E. Krause, R. Kron, K. Kuehn, N. Kuropatkin, O. Lahav, P. F. Leget, P. Lemos, A. R. Liddle, C. Lidman, M. Lima,

H. Lin, N. MacCrann, M. A. G. Maia, J. L. Marshall, P. Martini, J. McCullough, P. Melchior, J. Mena-Fernández, F. Menanteau, R. Miquel, J. J. Mohr, R. Morgan, J. Muir, J. Myles, S. Nadathur, A. Navarro-Alsina, R. C. Nichol, R. L. C. Ogando, Y. Omori, A. Palmese, S. Pandey, Y. Park, F. Paz-Chinchón, D. Petravick, A. Pieres, A. A. Plazas Malagón, A. Porredon, J. Prat, M. Raveri, M. Rodriguez-Monroy, R. P. Rollins, A. K. Romer, A. Roodman, R. Rosenfeld, A. J. Ross, E. S. Rykoff, S. Samuroff, C. Sánchez, E. Sanchez, J. Sanchez, D. Sanchez Cid, V. Scarpine, M. Schubnell, D. Scolnic, L. F. Secco, S. Serrano, I. Sevilla-Noarbe, E. Sheldon, T. Shin, M. Smith, M. Soares-Santos, E. Suchyta, M. E. C. Swanson, M. Tabbutt, G. Tarle, D. Thomas, C. To, A. Troja, M. A. Troxel, D. L. Tucker, I. Tutusaus, T. N. Varga, A. R. Walker, N. Weaverdyck, J. Weller, B. Yanny, B. Yin, Y. Zhang, and J. Zuntz, Dark Energy Survey Year 3 Results: Cosmological Constraints from Galaxy Clustering and Weak Lensing, arXiv e-prints, arXiv:2105.13549 (2021),

- arXiv:2105.13549 [astro-ph.CO].
- [8] S. Clesse and J. García-Bellido, Massive primordial black holes from hybrid inflation as dark matter and the seeds of galaxies, *Phys. Rev. D* **92**, 023524 (2015), arXiv:1501.07565 [astro-ph.CO].
- [9] J. García-Bellido and E. Ruiz Morales, Primordial black holes from single field models of inflation, *Physics of the Dark Universe* **18**, 47 (2017), arXiv:1702.03901 [astro-ph.CO].
- [10] C. T. Byrnes, P. S. Cole, and S. P. Patil, Steepest growth of the power spectrum and primordial black holes, *J. Cosmology Astropart. Phys.* **2019**, 028 (2019), arXiv:1811.11158 [astro-ph.CO].
- [11] D. J. H. Chung, E. W. Kolb, A. Riotto, and I. I. Tkachev, Probing planckian physics: Resonant production of particles during inflation and features in the primordial power spectrum, *Phys. Rev. D* **62**, 043508 (2000).
- [12] N. Barnaby and Z. Huang, Particle production during inflation: Observational constraints and signatures, *Phys. Rev. D* **80**, 126018 (2009).
- [13] N. Barnaby, Features and non-gaussianity from inflationary particle production, *Phys. Rev. D* **82**, 106009 (2010).
- [14] G. Barenboim and J. Rasero, Structure formation during an early period of matter domination, *Journal of High Energy Physics* **2014**, 138 (2014), arXiv:1311.4034 [hep-ph].
- [15] A. L. Erickcek and K. Sigurdson, Reheating effects in the matter power spectrum and implications for substructure, *Phys. Rev. D* **84**, 083503 (2011).
- [16] J. Fan, O. Özsoy, and S. Watson, Nonthermal histories and implications for structure formation, *Phys. Rev. D* **90**, 043536 (2014).
- [17] A. L. Erickcek, The dark matter annihilation boost from low-temperature reheating, *Phys. Rev. D* **92**, 103505 (2015).
- [18] K. Redmond, A. Trezza, and A. L. Erickcek, Growth of dark matter perturbations during kination, *Phys. Rev. D* **98**, 063504 (2018).
- [19] A. S. Josan and A. M. Green, Gamma rays from ultracompact minihalos: Potential constraints on the primordial curvature perturbation, *Yprd* **82**, 083527 (2010), arXiv:1006.4970 [astro-ph.CO].
- [20] P. Scott and S. Sivertsson, Gamma Rays from Ultracompact Primordial Dark Matter Minihalos, *Phys. Rev. Lett.* **103**, 211301 (2009), arXiv:0908.4082 [astro-ph.CO].
- [21] T. Bringmann, P. Scott, and Y. Akrami, Improved constraints on the primordial power spectrum at small scales from ultracompact minihalos, *Phys. Rev. D* **85**, 125027 (2012), arXiv:1110.2484 [astro-ph.CO].
- [22] H. A. Clark, G. F. Lewis, and P. Scott, Investigating dark matter substructure with pulsar timing - I. Constraints on ultracompact minihaloes, *Mnras* **456**, 1394 (2016), arXiv:1509.02938 [astro-ph.CO].
- [23] T. Nakama, T. Suyama, K. Kohri, and N. Hiroshima, Constraints on small-scale primordial power by annihilation signals from extragalactic dark matter minihalos, *Phys. Rev. D* **97**, 023539 (2018), arXiv:1712.08820 [astro-ph.CO].
- [24] M. S. Delos, A. L. Erickcek, A. P. Bailey, and M. A. Alvarez, Are ultracompact minihalos really ultracompact?, *Phys. Rev. D* **97**, 041303 (2018), arXiv:1712.05421 [astro-ph.CO].
- [25] M. S. Delos, A. L. Erickcek, A. P. Bailey, and M. A. Alvarez, Density profiles of ultracompact minihalos: Implications for constraining the primordial power spectrum, *Phys. Rev. D* **98**, 063527 (2018), arXiv:1806.07389 [astro-ph.CO].
- [26] D. Zhang, Impact of primordial ultracompact minihaloes on the intergalactic medium and first structure formation, *MNRAS* **418**, 1850 (2011), arXiv:1011.1935 [astro-ph.CO].
- [27] Y. Yang, L. Feng, X. Huang, X. Chen, T. Lu, and H. Zong, Constraints on ultracompact minihalos from extragalactic γ -ray background, *J. Cosmology Astropart. Phys.* **2011**, 020 (2011), arXiv:1112.6229 [astro-ph.CO].
- [28] Y. Yang, Contributions of dark matter annihilation within ultracompact minihalos to the 21 cm background signal, *European Physical Journal Plus* **131**, 432 (2016), arXiv:1612.06559 [astro-ph.CO].
- [29] H. A. Clark, N. Iwanus, P. J. Elahi, G. F. Lewis, and P. Scott, Heating of galactic gas by dark matter annihilation in ultracompact minihalos, *J. Cosmology Astropart. Phys.* **2017**, 048 (2017), arXiv:1611.08619 [astro-ph.CO].
- [30] G. Steigman and M. S. Turner, Cosmological constraints on the properties of weakly interacting massive particles, *Nuclear Physics B* **253**, 375 (1985).
- [31] G. Jungman, M. Kamionkowski, and K. Griest, Supersymmetric dark matter, *Phys. Rep.* **267**, 195 (1996), arXiv:hep-ph/9506380 [hep-ph].
- [32] E. W. Kolb, D. J. H. Chung, and A. Riotto, WIMPZILLAS!, in *Dark matter in Astrophysics and Particle Physics*, edited by H. V. Klapdor-Kleingrothaus and L. Baudis (1999) p. 592, arXiv:hep-ph/9810361 [hep-ph].
- [33] W. B. A. et al., THE LARGE AREA TELESCOPE ON THE *lessig*greaterFERMI GAMMA-RAY SPACE TELESCOPE *lessig*greaterMISSION, *The Astrophysical Journal* **697**, 1071 (2009).
- [34] F. Li, A. L. Erickcek, and N. M. Law, A new probe of the small-scale primordial power spectrum: Astrometric microlensing by ultracompact minihalos, *Yprd* **86**, 043519 (2012), arXiv:1202.1284 [astro-ph.CO].
- [35] K. Furugori, K. T. Abe, T. Tanaka, D. Hashimoto, H. Tashiro, and K. Hasegawa, The 21-cm signals from ultracompact minihaloes as a probe of primordial small-scale fluctuations, *MNRAS* **494**, 4334 (2020), arXiv:2002.04817 [astro-ph.CO].
- [36] K. T. Abe, T. Minoda, and H. Tashiro, Constraint on the early-formed dark matter halos using the free-free emission in the Planck foreground analysis, *Phys. Rev. D* **105**, 063531 (2022), arXiv:2108.00621 [astro-ph.CO].
- [37] K. T. Abe, Cosmological contribution from population III stars in ultracompact minihalos, *Phys. Rev. D* **106**, 083521 (2022), arXiv:2208.00375 [astro-ph.CO].
- [38] D. J. Fixsen, E. S. Cheng, J. M. Gales, J. C. Mather, R. A. Shafer, and E. L. Wright, The Cosmic Microwave Background Spectrum from the Full COBE FIRAS Data Set, *ApJ* **473**, 576 (1996), arXiv:astro-ph/9605054 [astro-ph].
- [39] J. C. Mather, E. S. Cheng, D. A. Cottingham, J. Eplee, R. E., D. J. Fixsen, T. Hewagama, R. B. Isaacman, K. A. Jensen, S. S. Meyer, P. D. Noerdlinger, S. M. Read, L. P. Rosen, R. A. Shafer, E. L. Wright, C. L. Bennett, N. W. Boggess, M. G. Hauser, T. Kelsall, J. Moseley, S. H., R. F. Silverberg, G. F. Smoot, R. Weiss, and D. T. Wilkinson, Measurement of the Cosmic Microwave Background Spectrum by the COBE FIRAS Instrument, *ApJ*

- 420**, 439 (1994).
- [40] R. Emami and G. F. Smoot, Observational constraints on the primordial curvature power spectrum, *J. Cosmology Astropart. Phys.* **2018**, 007 (2018), [arXiv:1705.09924 \[astro-ph.CO\]](#).
- [41] J. M. Bardeen, J. R. Bond, N. Kaiser, and A. S. Szalay, The Statistics of Peaks of Gaussian Random Fields, *ApJ* **304**, 15 (1986).
- [42] A. Lewis and A. Challinor, CAMB: Code for Anisotropies in the Microwave Background, Astrophysics Source Code Library, record ascl:1102.026 (2011), [ascl:1102.026](#).
- [43] A. Lewis and A. Challinor, Weak gravitational lensing of the CMB, *Phys. Rep.* **429**, 1 (2006), [arXiv:astro-ph/0601594 \[astro-ph\]](#).
- [44] P. A. R. Ade, Z. Ahmed, M. Amiri, D. Barkats, R. B. Thakur, C. A. Bischoff, D. Beck, J. J. Bock, H. Boenish, E. Bullock, V. Buza, J. R. Cheshire, J. Connors, J. Cornelison, M. Crumrine, A. Cukierman, E. V. Denison, M. Dierickx, L. Duband, M. Eiben, S. Fatigoni, J. P. Filippini, S. Fliescher, N. Goeckner-Wald, D. C. Goldfinger, J. Grayson, P. Grimes, G. Hall, G. Halal, M. Halpern, E. Hand, S. Harrison, S. Henderson, S. R. Hildebrandt, G. C. Hilton, J. Hubmayr, H. Hui, K. D. Irwin, J. Kang, K. S. Karkare, E. Karpel, S. A. Kefeli, S. A. Kernasovskiy, J. M. Kovac, C. L. Kuo, K. Lau, E. M. Leitch, A. Lennox, K. G. Megerian, L. Minutolo, L. Moncelsi, Y. Nakato, T. Namikawa, H. T. Nguyen, R. O’Brien, R. W. Ogburn, S. Palladino, T. Prouve, C. Pryke, B. Racine, C. D. Reintsema, S. Richter, A. Schillaci, R. Schwarz, B. L. Schmitt, C. D. Sheehy, A. Soliman, T. S. Germaine, B. Steinbach, R. V. Sudiwala, G. P. Teply, K. L. Thompson, J. E. Tolan, C. Tucker, A. D. Turner, C. Umiltà, C. Vergès, A. G. Vieregg, A. Wandui, A. C. Weber, D. V. Wiebe, J. Willmert, C. L. Wong, W. L. K. Wu, H. Yang, K. W. Yoon, E. Young, C. Yu, L. Zeng, C. Zhang, and S. Zhang (BICEP/Keck Collaboration), Improved constraints on primordial gravitational waves using planck, wmap, and bicep/keck observations through the 2018 observing season, *Phys. Rev. Lett.* **127**, 151301 (2021).
- [45] A. J. Mead, C. Heymans, L. Lombriser, J. A. Peacock, O. I. Steele, and H. A. Winther, Accurate halo-model matter power spectra with dark energy, massive neutrinos and modified gravitational forces, *MNRAS* **459**, 1468 (2016), [arXiv:1602.02154 \[astro-ph.CO\]](#).
- [46] U. Seljak, Analytic model for galaxy and dark matter clustering, *MNRAS* **318**, 203 (2000), [arXiv:astro-ph/0001493 \[astro-ph\]](#).
- [47] H. J. Mo, Y. P. Jing, and S. D. M. White, High-order correlations of peaks and haloes: a step towards understanding galaxy biasing, *MNRAS* **284**, 189 (1997), [astro-ph/9603039](#).
- [48] B. Diemer and A. V. Kravtsov, Dependence of the Outer Density Profiles of Halos on Their Mass Accretion Rate, *ApJ* **789**, 1 (2014), [arXiv:1401.1216 \[astro-ph.CO\]](#).
- [49] B. Diemer and M. Joyce, An Accurate Physical Model for Halo Concentrations, *ApJ* **871**, 168 (2019), [arXiv:1809.07326 \[astro-ph.CO\]](#).
- [50] T. Ishiyama, F. Prada, A. A. Klypin, M. Sinha, R. B. Metcalf, E. Jullo, B. Altieri, S. A. Cora, D. Croton, S. de la Torre, D. E. Millán-Calero, T. Oogi, J. Ruedas, and C. A. Vega-Martínez, The Uchuu Simulations: Data Release 1 and Dark Matter Halo Concentrations, *arXiv e-prints*, [arXiv:2007.14720 \(2020\)](#), [arXiv:2007.14720 \[astro-ph.CO\]](#).
- [51] E. Bertschinger, Self-similar secondary infall and accretion in an Einstein-de Sitter universe, *ApJS* **58**, 39 (1985).
- [52] B. Moore, T. Quinn, F. Governato, J. Stadel, and G. Lake, Cold collapse and the core catastrophe, *MNRAS* **310**, 1147 (1999), [arXiv:astro-ph/9903164 \[astro-ph\]](#).
- [53] J. T. Sayre, C. L. Reichardt, J. W. Henning, P. A. R. Ade, A. J. Anderson, J. E. Austermann, J. S. Avva, J. A. Beall, A. N. Bender, B. A. Benson, F. Bianchini, L. E. Bleem, J. E. Carlstrom, C. L. Chang, P. Chaubal, H. C. Chiang, R. Citron, C. Corbett Moran, T. M. Crawford, A. T. Crites, T. de Haan, M. A. Dobbs, W. Everett, J. Gallicchio, E. M. George, A. Gilbert, N. Gupta, N. W. Halverson, N. Harrington, G. C. Hilton, G. P. Holder, W. L. Holzapfel, J. D. Hrubes, N. Huang, J. Hubmayr, K. D. Irwin, L. Knox, A. T. Lee, D. Li, A. Lowitz, J. J. McMahon, S. S. Meyer, L. M. Mocaanu, J. Montgomery, A. Nadolski, T. Natoli, J. P. Nibarger, G. Noble, V. Novosad, S. Padin, S. Patil, C. Pryke, J. E. Ruhl, B. R. Saliwanchik, K. K. Schaffer, C. Sievers, G. Smecher, A. A. Stark, C. Tucker, K. Vanderlinde, T. Veach, J. D. Vieira, G. Wang, N. Whitehorn, W. L. K. Wu, V. Yefremenko, and SPTpol Collaboration, Measurements of B-mode polarization of the cosmic microwave background from 500 square degrees of SPTpol data, *Phys. Rev. D* **101**, 122003 (2020), [arXiv:1910.05748 \[astro-ph.CO\]](#).
- [54] C. L. Reichardt, S. Patil, P. A. R. Ade, A. J. Anderson, J. E. Austermann, J. S. Avva, E. Baxter, J. A. Beall, A. N. Bender, B. A. Benson, F. Bianchini, L. E. Bleem, J. E. Carlstrom, C. L. Chang, P. Chaubal, H. C. Chiang, T. L. Chou, R. Citron, C. C. Moran, T. M. Crawford, A. T. Crites, T. de Haan, M. A. Dobbs, W. Everett, J. Gallicchio, E. M. George, A. Gilbert, N. Gupta, N. W. Halverson, N. Harrington, J. W. Henning, G. C. Hilton, G. P. Holder, W. L. Holzapfel, J. D. Hrubes, N. Huang, J. Hubmayr, K. D. Irwin, L. Knox, A. T. Lee, D. Li, A. Lowitz, D. Luong-Van, J. J. McMahon, J. Mehl, S. S. Meyer, M. Millea, L. M. Mocaanu, J. J. Mohr, J. Montgomery, A. Nadolski, T. Natoli, J. P. Nibarger, G. Noble, V. Novosad, Y. Omori, S. Padin, C. Pryke, J. E. Ruhl, B. R. Saliwanchik, J. T. Sayre, K. K. Schaffer, E. Shirokoff, C. Sievers, G. Smecher, H. G. Spieler, Z. Staniszewski, A. A. Stark, C. Tucker, K. Vanderlinde, T. Veach, J. D. Vieira, G. Wang, N. Whitehorn, R. Williamson, W. L. K. Wu, and V. Yefremenko, An Improved Measurement of the Secondary Cosmic Microwave Background Anisotropies from the SPT-SZ + SPTpol Surveys, *ApJ* **908**, 199 (2021), [arXiv:2002.06197 \[astro-ph.CO\]](#).
- [55] J. W. Henning, J. T. Sayre, C. L. Reichardt, P. A. R. Ade, A. J. Anderson, J. E. Austermann, J. A. Beall, A. N. Bender, B. A. Benson, L. E. Bleem, J. E. Carlstrom, C. L. Chang, H. C. Chiang, H. M. Cho, R. Citron, C. Corbett Moran, T. M. Crawford, A. T. Crites, T. de Haan, M. A. Dobbs, W. Everett, J. Gallicchio, E. M. George, A. Gilbert, N. W. Halverson, N. Harrington, G. C. Hilton, G. P. Holder, W. L. Holzapfel, S. Hoover, Z. Hou, J. D. Hrubes, N. Huang, J. Hubmayr, K. D. Irwin, R. Keisler, L. Knox, A. T. Lee, E. M. Leitch, D. Li, A. Lowitz, A. Manzotti, J. J. McMahon, S. S. Meyer, L. Mocaanu, J. Montgomery, A. Nadolski, T. Natoli, J. P. Nibarger, V. Novosad, S. Padin, C. Pryke, J. E. Ruhl, B. R. Saliwanchik, K. K. Schaffer, C. Sievers, G. Smecher, A. A. Stark, K. T. Story, C. Tucker, K. Van-

- derlinde, T. Veach, J. D. Vieira, G. Wang, N. Whitehorn, W. L. K. Wu, and V. Yefremenko, Measurements of the Temperature and E-mode Polarization of the CMB from 500 Square Degrees of SPTpol Data, *ApJ* **852**, 97 (2018), [arXiv:1707.09353 \[astro-ph.CO\]](#).
- [56] S. Dahal, J. W. Appel, R. Datta, M. K. Brewer, A. Ali, C. L. Bennett, R. Bustos, M. Chan, D. T. Chuss, J. Cleary, J. D. Couto, K. L. Denis, R. Dünner, J. Eimer, F. Espinoza, T. Essinger-Hileman, J. E. Golec, K. Harrington, K. Helson, J. Iuliano, J. Karakla, Y. Li, T. A. Marriage, J. J. McMahon, N. J. Miller, S. Novack, C. Núñez, K. Osumi, I. L. Padilla, G. A. Palma, L. Parker, M. A. Petroff, R. Reeves, G. Rhoades, K. Rostem, D. A. N. Valle, D. J. Watts, J. L. Weiland, E. J. Wollack, and Z. Xu, Four-year Cosmology Large Angular Scale Surveyor (CLASS) Observations: On-sky Receiver Performance at 40, 90, 150, and 220 GHz Frequency Bands, *ApJ* **926**, 33 (2022), [arXiv:2107.08022 \[astro-ph.IM\]](#).
- [57] K. Lee, R. T. Génova-Santos, M. Hazumi, S. Honda, H. Kutsuma, S. Oguri, C. Otani, M. W. Peel, Y. Sueno, J. Suzuki, O. Tajima, and E. Won, A Forecast of the Sensitivity on the Measurement of the Optical Depth to Reionization with the GroundBIRD Experiment, *ApJ* **915**, 88 (2021), [arXiv:2102.03210 \[astro-ph.CO\]](#).
- [58] N. N. Gandilo *et al.* (PIPER), The Primordial Inflation Polarization Explorer (PIPER), *Proc. SPIE Int. Soc. Opt. Eng.* **9914**, 99141J (2016), [arXiv:1607.06172 \[astro-ph.IM\]](#).
- [59] M. Hazumi, P. A. R. Ade, A. Adler, E. Allys, K. Arnold, D. Auguste, J. Aumont, R. Aurlen, J. Austermann, C. Baccigalupi, A. J. Banday, R. Banjeri, R. B. Barreiro, S. Basak, J. Beall, D. Beck, S. Beckman, J. Bermejo, P. de Bernardis, M. Bersanelli, J. Bonis, J. Borrill, F. Boulanger, S. Bounissou, M. Brilenkov, M. Brown, M. Bucher, E. Calabrese, P. Campeti, A. Carones, F. J. Casas, A. Challinor, V. Chan, K. Cheung, Y. Chinone, J. F. Cliche, L. Colombo, F. Columbro, J. Cubas, A. Cukierman, D. Curtis, G. D'Alessandro, N. Dachlythra, M. De Petris, C. Dickinson, P. Diego-Palazuelos, M. Dobbs, T. Dotani, L. Duband, S. Duff, J. M. Duval, K. Ebisawa, T. Elleflot, H. K. Eriksen, J. Errard, T. Essinger-Hileman, F. Finelli, R. Flauger, C. Franceschet, U. Fuskeland, M. Galloway, K. Ganga, J. R. Gao, R. Genova-Santos, M. Gerbino, M. Gerbasi, T. Ghigna, E. Gjerløw, M. L. Gradziel, J. Grain, F. Grupp, A. Gruppuso, J. E. Gudmundsson, T. de Haan, N. W. Halverson, P. Hargrave, T. Hasebe, M. Hasegawa, M. Hattori, S. Henrot-Versillé, D. Herman, D. Herranz, C. A. Hill, G. Hilton, Y. Hirota, E. Hivon, R. A. Hlozek, Y. Hoshino, E. de la Hoz, J. Hubmayr, K. Ichiki, T. Iida, H. Imada, K. Ishimura, H. Ishino, G. Jaehnig, T. Kaga, S. Kashima, N. Katayama, A. Kato, T. Kawasaki, R. Keskitalo, T. Kisner, Y. Kobayashi, N. Kogiso, A. Kogut, K. Kohri, E. Komatsu, K. Komatsu, K. Konishi, N. Krachmalnicoff, I. Kreykenbohm, C. L. Kuo, A. Kushino, L. Lamagna, J. V. Lanen, M. Lattanzi, A. T. Lee, C. Leloup, F. Levrier, E. Linder, T. Louis, G. Luzzi, T. Maciaszek, B. Maffei, D. Maino, M. Maki, S. Mandelli, E. Martinez-Gonzalez, S. Masi, T. Matsumura, A. Mennella, M. Migliaccio, Y. Minami, K. Mitsuda, J. Montgomery, L. Montier, G. Morgante, B. Mot, Y. Murata, J. A. Murphy, M. Nagai, Y. Nagano, T. Nagasaki, R. Nagata, S. Nakamura, T. Namikawa, P. Natoli, S. Nerval, T. Nishibori, H. Nishino, F. Noviello, C. O'Sullivan, H. Ogawa, H. Ogawa, S. Oguri, H. Ohsaki, I. S. Ohta, N. Okada, N. Okada, L. Pagano, A. Paiella, D. Paoletti, G. Patanchon, J. Peloton, F. Piacentini, G. Pisano, G. Polenta, D. Poletti, T. Prouvé, G. Puglisi, D. Rambaud, C. Raun, S. Realini, M. Reinecke, M. Remazeilles, A. Ritacco, G. Roudil, J. A. Rubino-Martin, M. Russell, H. Sakurai, Y. Sakurai, M. Sandri, M. Sasaki, G. Savini, D. Scott, J. Seibert, Y. Sekimoto, B. Sherwin, K. Shinozaki, M. Shiraiishi, P. Shirron, G. Signorelli, G. Smecher, S. Stever, R. Stompor, H. Sugai, S. Sugiyama, A. Suzuki, J. Suzuki, T. L. Svalheim, E. Switzer, R. Takaku, H. Takakura, S. Takakura, Y. Takase, Y. Takeda, A. Tartari, E. Taylor, Y. Terao, H. Thommesen, K. L. Thompson, B. Thorne, T. Toda, M. Tomasi, M. Tominaga, N. Trappe, M. Tristram, M. Tsuji, M. Tsujimoto, C. Tucker, J. Ullom, G. Vermeulen, P. Vielva, F. Villa, M. Vissers, N. Vittorio, I. Wehus, J. Weller, B. Westbrook, J. Wilms, B. Winter, E. J. Wollack, N. Y. Yamasaki, T. Yoshida, J. Yumoto, M. Zannoni, and A. Zonca, LiteBIRD satellite: JAXA's new strategic L-class mission for all-sky surveys of cosmic microwave background polarization, in *Space Telescopes and Instrumentation 2020: Optical, Infrared, and Millimeter Wave*, Society of Photo-Optical Instrumentation Engineers (SPIE) Conference Series, Vol. 11443, edited by M. Lystrup and M. D. Perrin (2020) p. 114432F, [arXiv:2101.12449 \[astro-ph.IM\]](#).